Gold Bull (2014) 47:95–101
DOI 10.1007/s13404-013-0128-3

ORIGINAL PAPER

Hollow γ-Al_2O_3 microspheres as highly "active" supports for Au nanoparticle catalysts in CO oxidation

Jie Wang · Zhen-Hao Hu · Yu-Xin Miao · Wen-Cui Li

Published online: 5 December 2013

Abstract Consisted of closely packed nanoflakes, γ-Al_2O_3 hollow microspheres with ca. 4–6 μm in diameter, and 500–700 nm in shell thickness have been hydrothermally synthesized through utilizing $Al(NO_3)_3{\cdot}9H_2O$ as precursor, urea as precipitant agent and sulfate K_2SO_4, $(NH_4)_2SO_4$, or $KAl(SO_4)_2{\cdot}12H_2O$ as additive, followed by a calcination step. The samples were further characterized by thermogravimetric analysis, scanning electron microscope, x-ray powder diffraction, nitrogen adsorption, and in situ diffuse reflectance infrared Fourier transform spectroscopy (DRIFTS) of adsorbed CO etc. The morphology of alumina products was strongly dependent on the presence of SO_4^{2-}. Then via a deposition–precipitation method, 3 wt.% Au nanoparticles supported on γ-Al_2O_3 hollow microspheres exhibit excellent performance with a complete CO conversion at 0 °C ($T_{100\%}$=0 °C) and 50 % conversion at −25 °C ($T_{50\%}$=−25 °C). The good catalytic activity is associated with the special hollow microsphere structures assembled by nanoflakes of γ-Al_2O_3 support. The DRIFTS confirms the presence of $Au^{\delta+}$ and Au^0 on the surface of γ-Al_2O_3 hollow microspheres. As a contrast, Au catalyst prepared using alumina support with undefined morphology shows low activity under the same catalytic test conditions ($T_{100\%}$=190 °C, $T_{50\%}$=80 °C).

Keywords Hollow microspheres · γ-Al_2O_3 · Au catalyst · CO oxidation

J. Wang · Z.-H. Hu · Y.-X. Miao · W.-C. Li (✉)
State Key Laboratory of Fine Chemicals, School of Chemical Engineering, Dalian University of Technology, Dalian 116024, People's Republic of China
e-mail: wencuili@dlut.edu.cn

Introduction

In the past decades, considerable attention has been paid to the supported gold catalysts for CO oxidation at low temperatures [1]. Various oxides, such as TiO_2 [2], Fe_2O_3 [3], Al_2O_3 [4–6], CeO_2 [7], MnO_x [8] etc., have been employed to disperse and stabilize Au nanoparticles. Thereinto, gold catalysts supported on reducible metal oxides, in particular on CeO_2, TiO_2, Fe_2O_3, MnO_x, are well known for their high activity for CO oxidation at low temperatures.

Among those nonreducible oxide supporting gold nanoparticles, Au/γ-Al_2O_3 is still a very interesting system for both practical application and academic study due to the extraordinary advantages of γ-Al_2O_3 such as high surface area and good mechanical and especially thermal, chemical stability [9]. However, the less active of Au/Al_2O_3 catalyst for CO oxidation has been observed experimentally. For example, gold nanoparticles supported on mesoporous γ-Al_2O_3 give a complete CO conversion when the reaction is performed at 150 °C [10]. When using commercial γ-Al_2O_3 support, the CO conversion of Au catalyst was only ca. 50 % at 65 °C ($T_{50\%}$) and reached to 90 % at 100 °C. Even after Au nanoparticles supported on γ-Al_2O_3nanofibers, the enhanced catalytic activity can only achieve the complete CO conversion at 40 °C ($T_{100\%}$=40 °C) [11]. Thus, it remains a grand challenge to obtain highly active Au/Al_2O_3 catalyst for CO oxidation. Recently, we reported the γ-$Al_2O_3$with thin sheets and rough surface acted as an extraordinary catalyst support for the stabilization of gold nanoparticles from sintering [4]. It reveals that, apart from its intrinsic quality, the morphology of support material plays a significant role in the reactive activity of Au catalysts.

Herein, assembled from closely packed nanoflakes, γ-Al_2O_3 hollow microsphere structures with ca. 4–6 μm in diameter and 500–700 nm in shell thickness have been hydrothermally prepared through adjusting the molar ratio of

Al^{3+} and SO_4^{2-}, followed by a calcination step. As such unique structures of γ-Al_2O_3 support could efficiently stabilize Au nanoparticles, the obtained Au catalyst exhibits extraordinarily high activity towards CO oxidation, where a complete CO conversion at 0 °C was achieved ($T_{50\%}$= −25 °C). This work could be distinguished by special hollow microspheres structures assembled by nanoflakes of γ-Al_2O_3 support and excellent catalytic activity for CO removal.

Experimental

Synthesis of Au/Al_2O_3 catalysts

Typically, aluminum nitrate, sulfates (K_2SO_4, $(NH_4)_2SO_4$ or $KAl(SO_4)_2{\cdot}12H_2O$) and urea were dissolved in 100-mL deionized water. The obtained mixture was transferred into a 150-mL Teflon-lined stainless steel autoclave and heated at 180 °C for 3 h. Then, the white precipitates were washed with deionized water and dried at 80 °C. The hydrothermally synthesized and dried samples were denoted as *Al_2O_3-x-hydro* (where x=1, 2, and 3, corresponding to different sulfate). After a calcination step at 500 °C for 2 h, the final products were obtained and named as *Al_2O_3-x*. The concentration of Al^{3+} was fixed as 0.05 M. The detail synthesis conditions and textural parameters were listed in Table 1. For comparison, alumina (denoted as *Al_2O_3-4*) was synthesized by a common precipitation method using aluminum nitrate as precursor and ammonium carbonate as precipitant.

Preparation of Au/Al_2O_3 catalyst and catalytic test

Au nanoparticles were deposited on the surface of the sample *Al_2O_3-x* (x=1, 2, 3, and 4) by a deposition–precipitation method with $HAuCl_4$ solution (7.9 g L^{-1}) at pH 8–9 in 60 °C for 2 h. After washing and drying, the precipitants were thermal treated at 250 °C for 2 h in the air to generate the Au/Al_2O_3 catalysts, denoted as *Au-(Al_2O_3-x)*. The Au content was theoretically estimated as 3 wt.%. The activity of Au catalysts for CO oxidation was evaluated in a fixed bed quartz reactor using 50 mg of catalyst (20–40 mesh) with a composition of 1 vol.% CO, 20 vol.% O_2, and 79 vol.% N_2 and the total rate of feed gas was 67 mL min^{-1} (80,000 mL h^{-1} g_{cat}^{-1}). The products were analyzed using a GC-7890 gas chromatograph equipped with a thermal conductivity detector.

Characterization

Thermogravimetric and differential scanning calorimetry analysis (TG-DSC) were conducted on a thermogravimetric analyzer STA 449 F3 (NETZSCH) under an air atmosphere with a heating rate of 10 °C min^{-1}. X-ray diffraction patterns (XRD) were obtained with a D/MAX-2400 diffractometer using Cu K_α radiation (40 kV, 100 mA, λ=1.54056 Å). Nitrogen adsorption/desorption isotherms were measured with a TriStar 3000 adsorption analyzer (Micromeritics) at liquid nitrogen temperature. The samples were degassed at 200 °C for 4 h prior to analysis. The Brunauer–Emmett–Teller (BET) method was used to calculate the specific surface areas (S_{BET}). Pore size distributions (PSDs) were derived from the desorption branches of the isotherms using the Barrett–Joyner–Halenda model. Scanning electron microscope (SEM) images were obtained with a Hitachi S-4800 instrument. Transmission electron microscope (TEM) images were obtained with a Tecnai G220 S-Twin microscope with accelerative voltage of 200 kV. The remained K and S contents were analyzed using an inductively coupled plasma atomic emission spectrometer (ICP-AES) on the Optima 2000 DV. Infrared Fourier transform spectra (FT-IR) were recorded using a Nicolet 6700 FT-IR spectrometer at a resolution of 4 cm^{-1} and scale at 4,000–640 cm^{-1}. Diffuse reflectance infrared Fourier transform spectra were recorded using a Nicolet 6700 FT-IR spectrometer at a resolution of 4 cm^{-1} and scale at 4,000–640 cm^{-1}. Self-supporting disks were prepared from the sample powders and treated directly in the IR cell. The catalysts were connected to a vacuum-adsorption apparatus with a residual pressure below 10^{-3} Pa. Prior to the CO adsorption (25 °C, 5 vol.% CO and N_2 in balance), the catalysts were evacuated for 30 min for 1 h at 100 °C.

Table 1 Synthesis conditions and structure parameters of γ-Al_2O_3 samples

Sample	Al^{3+} precursor	Sulfate	Precipitant agent	S_{BET} (m^2 g^{-1})	V_{total} (cm^3 g^{-1})	D_{peak} (nm)
Al_2O_3-1	$Al(NO_3)_3{\cdot}9H_2O$	K_2SO_4	$CO(NH_2)_2$	186	0.74	4/14
Al_2O_3-2	$Al(NO_3)_3{\cdot}9H_2O$	$(NH_4)_2SO_4$	$CO(NH_2)_2$	187	0.74	4/17
Al_2O_3-3	$KAl(SO_4)_2{\cdot}12H_2O$	$KAl(SO_4)_2{\cdot}12H_2O$	$CO(NH_2)_2$	209	0.66	3
Al_2O_3-4	$Al(NO_3)_3{\cdot}9H_2O$	–	$(NH_4)_2CO_3$	268	0.92	19

S_{BET} specific surface area calculated by the Brunauer–Emmett–Teller (BET) method, V_{total} total pore volumes at P/P_0=0.997, D_{peak} pore sizes at maxima of the pore size distributions (PSDs)

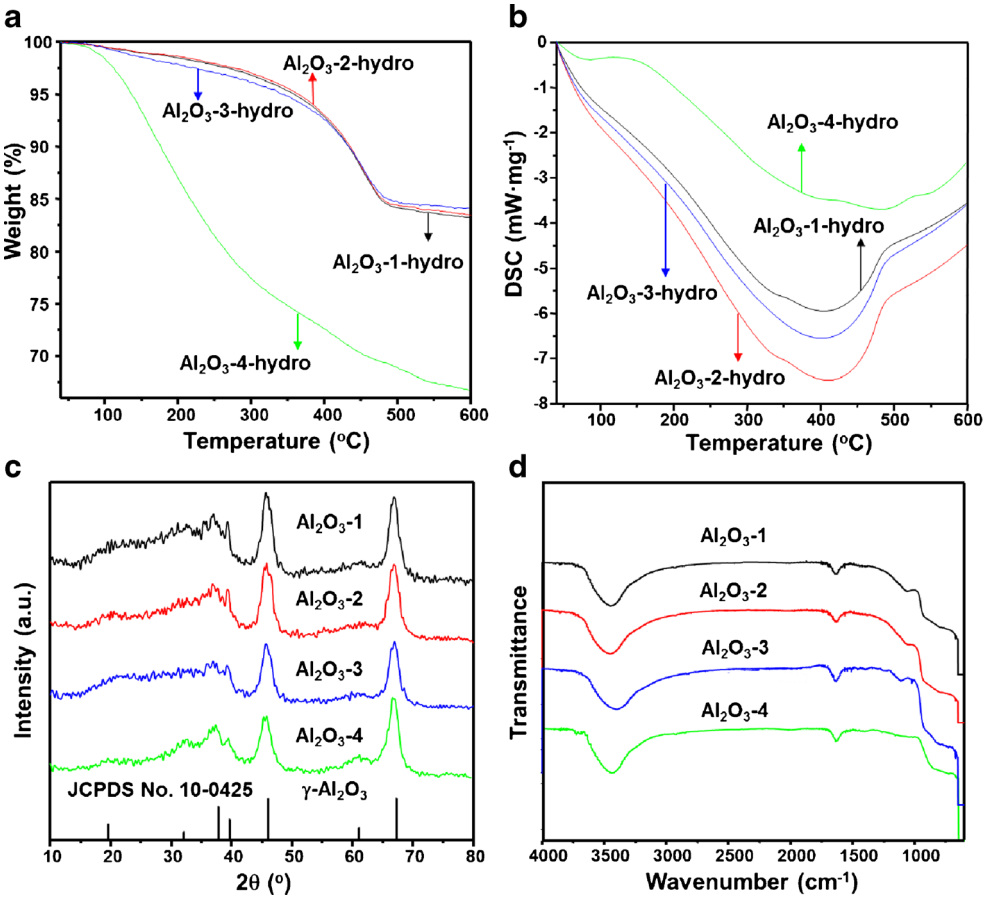

Fig. 1 **a** TG and **b** DSC curves of hydrothermal products (without calcination), **c** XRD patterns and **d** FT-IR curves of alumina supports (calcined at 500 °C for 2 h)

Results and discussion

Alumina hollow microspheres

To explore the thermal decomposition behavior, hydrothermal products were characterized by TG-DSC (Fig. 1a, b) under air, with a heating rate of 10 °C min^{-1}. In the case of samples *Al_2O_3-x-hydro* (x=1, 2, and 3), the TG curves show a sharp weight loss before 470 °C with the actual loss is ~18 %, mainly corresponding the release of adsorbed water and the decomposition of AlO(OH) ($2AlO(OH) \rightarrow Al_2O_3 + H_2O$, theory weight loss value is ~15 %) [12]. The DSC curve displays a broad exothermic peak at 420 °C, which indicates the phase conversion. We thus selected 500 °C as the calcination temperature. However, Al_2O_3-4-hydro sample shows the weight loss of ~34 % below 600 °C, which is corresponding to the intermediate product $Al(OH)_3$ ($2Al(OH)_3 \rightarrow Al_2O_3 + 3H_2O$, theory weight loss value is ~34.6 %) [13].

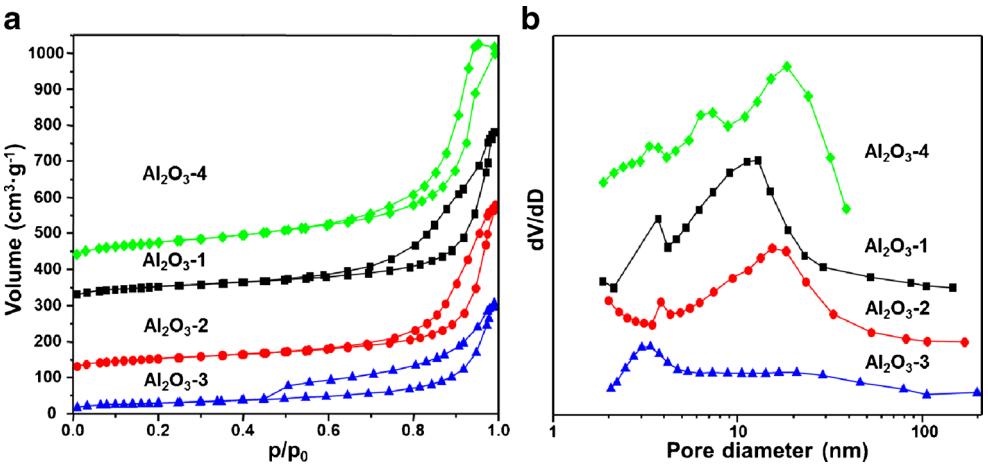

Fig. 2 **a** N_2 sorption isotherms and **b** pore size distributions of *Al_2O_3-1*, *Al_2O_3-2*, *Al_2O_3-3* and *Al_2O_3-4* aluminas. The isotherms of *Al_2O_3-4*, *Al_2O_3-1* and *Al_2O_3-2* were offset up by 400, 300, and 100 cm^3 g^{-1}

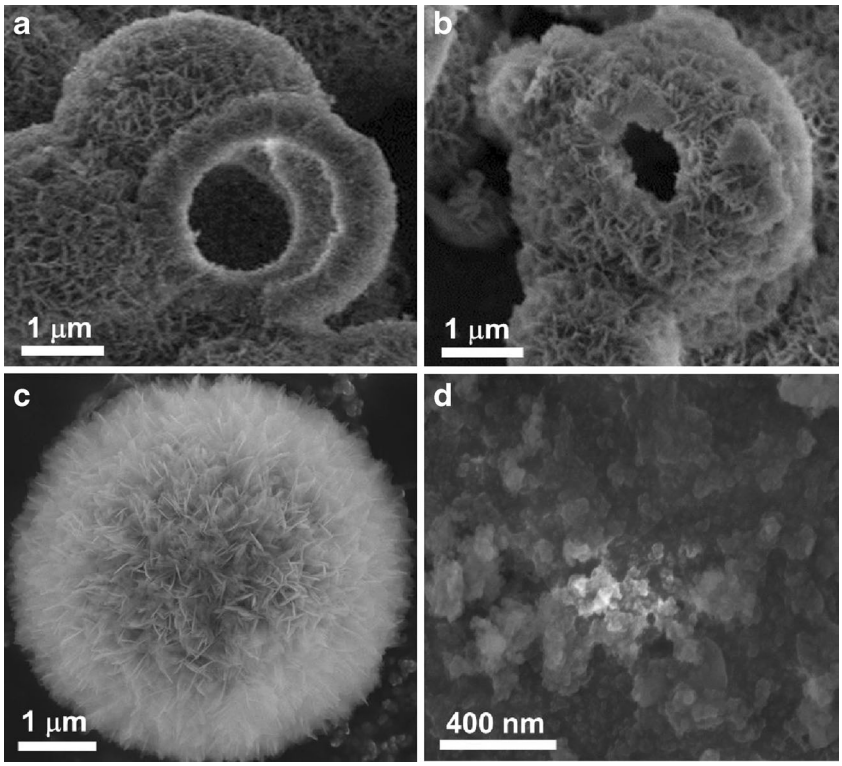

Fig. 3 SEM images of alumina supports (**a** Al_2O_3-*1*, **b** Al_2O_3-*2*, **c** Al_2O_3-*3*, **d** Al_2O_3-*4*)

Based on the XRD analysis results in Fig. 1c, all the diffraction peaks of calcined samples Al_2O_3-*x* (x=1, 2, 3, and 4) can be assigned to γ-Al_2O_3 (JCPDS No. 10-0425). According to the Scherrer equation, the crystallite size of nanoflake composed hollow microsphere is ca. 13, 10, 12, and 10 nm for Al_2O_3-*1*, Al_2O_3-*2*, Al_2O_3-*3*, and Al_2O_3-*4*, respectively. More characteristics were detected in the FT-IR spectra (Fig. 1d). Basically, four samples show similar IR signals. The intensive bands at 3,447–3,449 and 1,637–1,638 cm^{-1} belong to the stretching and bending vibrations of the O–H bonds adjoining the Al atoms and a functional group of water [14–16]. The intensive peaks at 1,160 and 1,070 cm^{-1} are due to the δ_{as} Al-O-H and δ_s Al-O-H modes, and the bands observed at 746 cm^{-1} represent the stretching modes of AlO_6 [17].

After annealing at 500 °C for 2 h, the alumina materials were further characterized by N_2 sorption measurements. As seen in Fig. 2, the nitrogen sorption isotherms of Al_2O_3-*1*, Al_2O_3-*2*, Al_2O_3-*3*, and Al_2O_3-*4* are essentially of type IV [18], reflecting a mesoporous characteristic. Determined from desorption branches, the pore size distributions of Al_2O_3-*1*, Al_2O_3-*2*, and Al_2O_3-*3* are centered at 4/17, 4/17, and 3 nm, whereas Al_2O_3-*4* shows a rather broad distribution with mesopore size concentrated at 19 nm. Al_2O_3-*4* exhibits a slightly higher BET surface area (268 m^2 g^{-1}) and total pore volume (0.92 m^3 g^{-1}) than those of Al_2O_3-*3* (209 and 0.66 m^3 g^{-1},

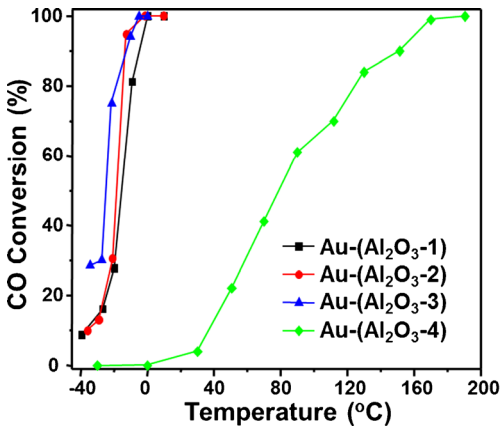

Fig. 4 CO conversion curves of gold catalysts *Au*-(Al_2O_3-*1*), *Au*-(Al_2O_3-*2*), *Au*-(Al_2O_3-*3*) and *Au*-(Al_2O_3-*4*)

Table 2 Catalytic activity of gold nanoparticles supported on different alumina

Gold catalyst	Au content (%)[a]	$T_{100\%}$ (°C)[b]	$T_{50\%}$ (°C)[b]	Rate (mol h^{-1} g_{Au}^{-1})[c]
Au-(Al_2O_3-1)	2.8	0	−15	1.267
Au-(Al_2O_3-2)	2.6	−1	−18	1.352
Au-(Al_2O_3-3)	2.6	0	−25	1.413
Au-(Al_2O_3-4)	2.7	190	80	–

[a] The actual Au content was detected by ICP technique

[b] $T_{50\%}$ and $T_{100\%}$ represent the temperatures for 50 and 100 % CO conversion, respectively

[c] The corresponding reactive rate of Au catalysts at 0 °C

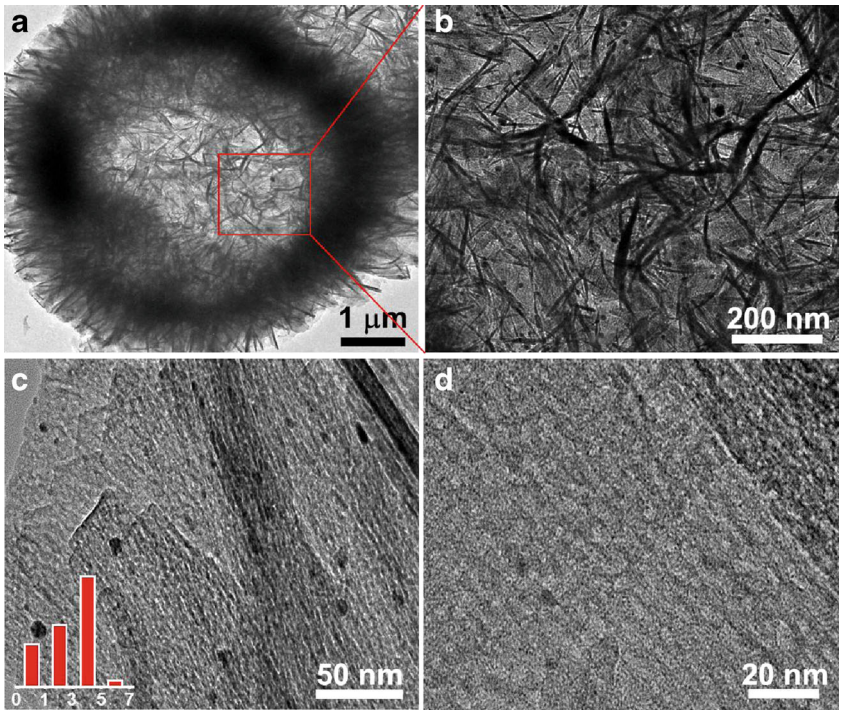

Fig. 5 TEM images of gold catalyst *Au-(Al_2O_3-3)* and size distribution of gold nanoparticles

accordingly). The detail structure parameters of γ-Al_2O_3 materials are listed in Table 1.

In addition, the morphologies of alumina were characterized by SEM technique. It can be clearly seen in Fig. 3a, b that *Al_2O_3-1* and *Al_2O_3-2* samples display hollow microsphere structures (the diameter ~4 μm and shell thickness 500–600 nm) with open mouths assembled from closely packed nanoflakes. When $KAl(SO_4)_2{\cdot}12H_2O$ was used as alumina precursor and sulfate additive (keeping the molar ratio of $Al:SO_4^{2-}=1:2$), then, the perfect γ-Al_2O_3 hollow microspheres with ca. 6 μm in diameter, 600–700 nm in shell thickness can be obtained (Fig. 3c). Whereas, *Al_2O_3-4* has an undefined morphology (Fig. 3d), which is totally different from alumina hollow microspheres prepared with the addition of sulfates. As the promotion of SO_4^{2-}, Al^{3+} and urea can alternatively hydrolyze and polycondense, which leads to the precipitation of amorphous aluminum oxyhydroxide spheres [18–23]. It can be deduced that the increase in concentration of SO_4^{2-} facilitates formation of larger microspheres through secondary nucleation and growth of AlO(OH) crystal nuclei until the system reaches equilibrium with the surrounding solution. It confirms that the sulfate anion plays a significant role in the formation of hollow microspheres morphology.

Au/Al_2O_3 catalyst for CO oxidation

As a simple and typical probe reaction, CO oxidation was selected to identify the promotion of γ-Al_2O_3 with unique hollow microspheres morphology assembled by closely packed nanoflakes for the catalytic performance of Au nanoparticle catalysts. Supported on obtained γ-Al_2O_3 hollow microspheres, the catalytic activity of 3 wt.% Au/Al_2O_3 catalysts were shown in Fig. 4 and Table 2.

Remarkably, the corresponding Au catalysts exhibited excellent catalytic performance with a complete CO conversion at ~0 °C. Particularly in the case of sample *Au-(Al_2O_3-3)*, the 50 % CO conversion can be achieved at −25 °C, and the specific rate at 0 °C was calculated as 1.413 mol h^{-1} g_{Au}^{-1}. For comparison, the regular Al_2O_3 support (*Al_2O_3-4*) with undefined morphology was synthesized by a common precipitation method using $Al(NO_3)_3{\cdot}9H_2O$ and $(NH_3)_4CO_3$. The obtained *Au-(Al_2O_3-4)* catalyst tested under the same conditions is generally inactive at 0 °C. The results in turn indicate

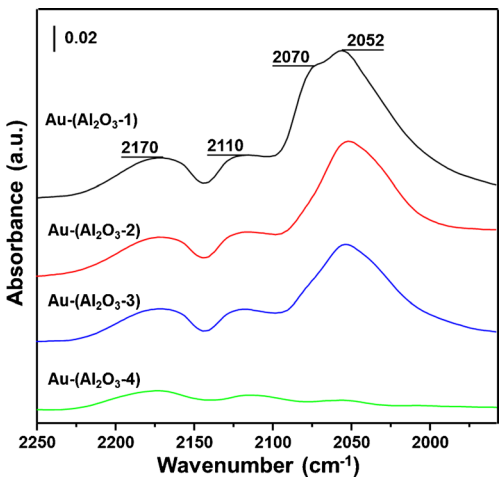

Fig. 6 In situ DRIFTS spectra of gold catalysts *Au-(Al_2O_3-1)*, *Au-(Al_2O_3-2)*, *Au-(Al_2O_3-3)* and *Au-(Al_2O_3-4)*

that such γ-Al_2O_3 hollow microspheres can efficiently stabilize Au nanoparticles, which exhibit higher catalytic performance for CO oxidation. In addition, despite the different catalytic test conditions, such as the composition of feed gas, the loading content of gold particles, and the temperature of calcination, the rate values in this work are comparable and even higher to the results in literatures [10, 13, 24–27].

Presently, from SEM images (Fig. 3) we know Al_2O_3-1, Al_2O_3-2, and Al_2O_3-3 have quite similar morphologies while Al_2O_3-4, as controlled sample, is in another case. On the other hand, the activity of Au/Al_2O_3-1, Au/Al_2O_3-2, and Au/Al_2O_3-3 samples are also quite similar in CO oxidation, while Au/Al_2O_3-4 shows a very low activity (Fig. 4). The Au contents of all samples were maintained nearly same (Table 2). Therefore, one representative sample Au/Al_2O_3-3 was characterized by TEM. As shown in Fig. 5a, b, gold catalysts supported on the surface of γ-Al_2O_3 hollow microspheres consisted of closely packed nanoflakes. Besides, Au nanoparticles are highly dispersed with an average size of 3.0±0.5 nm estimated from the TEM images in Fig. 5c. In addition, Fig. 5d shows a rough surface of γ-Al_2O_3 hollow microspheres, which are beneficial to stabilize gold nanoparticles efficiently. From our previous work [13], the controlled sample Au/Al_2O_3-4 has a gold particle size of 2.5±0.5 nm based on the TEM observation, which is more or less similar to that of sample Au/Al_2O_3-3. All these information demonstrates the advantages of the rough surface of γ-Al_2O_3 hollow microspheres. Furthermore, concerning the influence of the possible remained heteroatoms (for example, sulfur and potassium) on the activity [28–30], sulfur contents and potassium contents of samples *Al_2O_3-1*, *Al_2O_3-2* and *Al_2O_3-3* were analyzed by ICP-AES technique, correspondingly. All three samples show ignorable sulfur and potassium content. Therefore, one can basically eliminate the influence of sulfate and K^+ on the catalytic performance. It further suggests that the shape and surface property of γ-Al_2O_3 support have strong influence on the activity of the Au nanoparticles.

To further explore the surface chemical property of Au nanoparticles on γ-Al_2O_3 hollow microsphere supports, in situ DRIFTS was applied to measure the adsorbed CO. As shown in Fig. 6, the strong absorption bands of CO positioned around 2,110 and 2,070 cm^{-1} appeared on the Au/Al_2O_3 samples dispersed on γ-Al_2O_3 hollow microspheres which belong to two linear CO species adsorbed on the metallic Au sites [31]. The peak at 2,170 cm^{-1} was attributed to CO adsorbed on cationic gold (Au(I) or Au(III)) [32]. The DRIFTS measurements suggest that the presence of $Au^{\delta+}$ and Au^0 on the surface of Au/Al_2O_3 catalysts, although weaker absorption bands were observed for Au nanoparticles supported on alumina *Al_2O_3-4*. Meanwhile, the absorption band appeared at 2,052 cm^{-1}, which can be assigned to CO adsorbed on a negatively charged gold surface [33]. Apparently, *Al_2O_3-4* synthesized by the common precipitation method displays an inferior surface for CO adsorption and thus results in a catalyst with a low catalytic activity.

Conclusions

It has been demonstrated that AlO(OH) hollow microspheres consist of closely packed nanoflakes were synthesized through a hydrothermal process by using $Al(NO_3)_3 \cdot 9H_2O$ as a precursor, urea as precipitant agent and sulfate K_2SO_4, $(NH_4)_2SO_4$, and $KAl(SO_4)_2 \cdot 12H_2O$ as additive. When adjusting the molar ratio of Al^{3+} and SO_4^{2-} to 1:2, γ-Al_2O_3 hollow microspheres with ca. 4–6 μm in diameter, 500–700 nm in shell thickness can be obtained after a calcination step. As such, γ-Al_2O_3 supports with special morphology and rough surface can stabilize gold nanoparticles efficiently; an excellent catalytic performance for CO oxidation can be achieved with a complete CO conversion at 0 °C and 50 % conversion at −25 °C. The DRIFTS confirms the presence of $Au^{\delta+}$ and Au^0 on the surface of Au/Al_2O_3 catalysts. In contrast, Au catalyst on alumina support with undefined morphology shows low activity at low temperature under the same catalytic test conditions.

Acknowledgments The project was supported by the National Natural Science Foundation of China (No.20973031) and the Ph.D. Programs Foundation (20100041110017) of Ministry of Education of China.

References

1. Haruta M, Kobayashi T, Sano H, Yamada N (1987) Novel gold catalysts for the oxidation of carbon monoxide at a temperature far below 0 °C. Chem Lett 16:405–408
2. Li WC, Comotti M, Schüth F (2006) Highly reproducible syntheses of active Au/TiO_2 catalysts for CO oxidation by deposition-precipitation or impregnation. J Catal 237:190–196
3. Herzing AA, Kiely CJ, Carley AF, Landon P, Hutchings GJ (2008) Identification of active gold nanoclusters on iron oxide supports for CO oxidation. Science 321:1331–1335
4. Wang J, Lu AH, Li MR, Zhang WP, Chen YS, Tian DX, Li WC (2013) Thin porous alumina sheets as supports for stabilizing gold nanoparticles. ACS Nano 7:4902–4910
5. Qi CX, Su HJ, Guan RG, Xu XF (2012) An investigation into phosphate-doped Au/alumina for low temperature CO oxidation. J Phys Chem C 116:17492–17500
6. Costello CK, Kung MC, Oh HS, Wang Y, Kung HH (2002) Nature of the active site for CO oxidation on highly active Au/γ-Al_2O_3. Appl Catal A Gen 232:159–168
7. Yang J, Wang FF, Ma XM, Tang QH, Wang K, Guo YM, Yang L (2013) Facile one-step synthesis of porous ceria hollow nanospheres for low temperature CO oxidation. Micropor Mesopor Mat 176:1–7

8. Frey K, Iablokov V, Sáfrán G, Osán J, Sajó I, Szukiewicz R, Chenakin S, Kruse N (2012) Nanostructured MnO_x as highly active catalyst for CO oxidation. J Catal 287:30–36
9. Comotti M, Li WC, Spliethoff B, Schüth F (2006) Support effect in high activity gold catalysts for CO oxidation. J Am Chem Soc 128: 917–924
10. Yuan Q, Duan HH, Li LL, Li ZX, Duan WT, Zhang LS, Song WG, Yan CH (2010) Homogeneously dispersed ceria nanocatalyst stabilized with ordered mesoporous alumina. Adv Mater 22:1475–1478
11. Han YF, Zhong Z, Ramesh K, Chen F, Chen L (2007) Effects of different types of γ-Al_2O_3 on the activity of gold nanoparticles for CO oxidation at low-temperatures. J Phys Chem C 111:3163–3170
12. Cai WQ, Yu JG, Jaroniec M (2010) Template-free synthesis of hierarchical spindle-like γ-Al_2O_3 materials and their adsorption affinity towards organic and inorganic pollutants in water. J Mater Chem 20:4587–4594
13. An AF, Lu AH, Sun Q, Wang J, Li WC (2011) Gold nanoparticles stabilized by a flake-like Al_2O_3 support. Gold Bull 44:217–222
14. Ahmad AL, Mustafa NNN (2007) Sol-gel synthesized of nanocomposite palladium–alumina ceramic membrane for H_2 permeability: preparation and characterization. Int J Hydrogen Energ 32:2010–2021
15. Liu F, Asakura K, He H, Shan W, Shi X, Zhang C (2011) Influence of sulfation on iron titanate catalyst for the selective catalytic reduction of NO_x with NH_3. Appl Catal B Environ 103:369–377
16. Romero-Pascual E, Larrea A, Monzón A, González RD (2002) Thermal stability of Pt/Al_2O_3 catalysts prepared by sol-gel. J Solid State Chem 168:343–353
17. Feng YL, Lu WC, Zhang LM, Bao XH, Yue BH, Lv Y, Shang XF (2008) One-step synthesis of hierarchical cantaloupe-like AlOOH superstructures via a hydrothermal route. Cryst Growth Des 8: 1426–1429
18. Yu JG, Liu W, Yu HG (2008) A one-pot approach to hierarchically nanoporous titania hollow microspheres with high photocatalytic activity. Cryst Growth Des 8:930–934
19. Yu HG, Yu JG, Liu SW, Mann S (2007) Template-free hydrothermal synthesis of CuO/Cu_2O composite hollow microspheres. Chem Mater 19:4327–4334
20. Matijevic E (1981) Monodispersed metal (hydrous) oxides—a fascinating field of colloid science. Acc Chem Res 14:22–29
21. Castellano M, Matijevic E (1989) Uniform colloidal zinc compounds of various morphologies. Chem Mater 1:78–82
22. Ramanathan S, Roy SK, Bhat R, Upadhyaya DD, Biswas AR (1997) Alumina powders from aluminium nitrate-urea and aluminium sulphate-urea reactions—the role of the precursor anion and process conditions on characteristics. Ceram Int 23:45–53
23. Zhou JB, Wang L, Zhang Z, Yu JG (2013) Facile synthesis of alumina hollow microspheres via trisodium citrate-mediated hydrothermal process and their adsorption performances for p-nitrophenol from aqueous solutions. J Colloid Interface Sci 394:509–514
24. Wang GH, Li WC, Jia KM, Spliethoff B, Schüth F, Lu AH (2009) Shape and size controlled α-Fe_2O_3 nanoparticles as supports for gold-catalysts: synthesis and influence of support shape and size on catalytic performance. Appl Catal A Gen 364:42–47
25. Kung HH, Kung MC, Costello CK (2003) Supported Au catalysts for low temperature CO oxidation. J Catal 216:425–432
26. Okumura M, Nakamura S, Tsubota S, Nakamura T, Azuma M, Haruta M (1998) Chemical vapor deposition of gold on Al_2O_3, SiO_2, and TiO_2 for the oxidation of CO and of H_2. Catal Lett 51: 53–58
27. Calla JT, Bore MT, Datye AK, Davis RJ (2006) Effect of alumina and titania on the oxidation of CO over Au nanoparticles evaluated by ^{13}C isotopic transient analysis. J Catal 238:458–467
28. Moma JA, Scurrell MS, Jordaan WA (2007) Effects of incorporation of ions into Au/TiO_2 catalysts for carbon monoxide oxidation. Top Catal 44:167–172
29. Solsona B, Conte M, Cong Y, Carley A, Hutchings G (2005) Unexpected promotion of Au/TiO_2 by nitrate for CO oxidation. Chem Commun 2351–2353
30. Mohapatra P, Moma J, Parida KM, Jordaan WA, Scurrell MS (2007) Dramatic promotion of gold/titania for CO oxidation by sulfate ions. Chem Commun 1044–1046
31. Somodi F, Borbáth I, Hegedűs M, Lázár K, Sajó IE, Geszti O, Rojas S, Fierro JLG, Margitfalvi JL (2009) Promoting effect of tin oxides on alumina-supported gold catalysts used in CO oxidation. Appl Surf Sci 256:726–736
32. Venkov T, Klimev H, Centeno MA, Odriozola JA, Hadjiivanov K (2006) State of gold on an Au/Al_2O_3 catalyst subjected to different pre-treatments: an FTIR study. Catal Commun 7:308–313
33. Liu X, Liu MH, Luo YC, Mou CY, Lin SD, Cheng H, Chen JM, Lee JF, Lin TS (2012) Strong metal-Support interactions between gold nanoparticles and ZnO nanorods in CO oxidation. J Am Chem Soc 134:10251–10258